J. Fluid Mech. (1991), *vol.* 224, *pp.* 117–132
Printed in Great Britain

The separated flow past a cylinder in a rotating frame

By ANNE BECKER
Department of Mathematics, Monash University, Clayton, Victoria 3168, Australia

(Received 17 November 1989 and in revised form 3 July 1990)

In this paper a numerical model for the viscous flow past a cylinder in a rotating frame is discussed when both the Rossby number Ro and Ekman number E are small. The results of this model are analysed and compared to an inviscid study by Page (1987) applicable in the limit $E \to 0$ with $Ro = O(E^{\frac{1}{2}})$. The detailed structure of the separated flow is also examined and compared to the proposals for the higher-order flow in $E^{\frac{1}{4}}$ layers in Page (1987) which were based, in part, on the theory of Smith (1979, 1985) for the non-rotating flow past bluff bodies. Some discrepancies between this theory and the numerical results are noted.

1. Introduction

The flow of a homogeneous, incompressible, viscous fluid past a right circular cylinder forms one of the classical problems of fluid dynamics. It has been studied by numerous workers since the latter half of the last century and still presents a challenge despite its apparent simplicity. A wealth of literature exists on this subject as well as several review articles, for example Morkovin (1964) and Berger & Wille (1972). When the flow takes place in a homogeneous fluid relative to a rotating frame of reference, a new series of flow phenomena emerge. Owing to the importance of background rotation on geophysical motions, such a system is of interest to meteorologists and oceanographers, and others studying topographic effects in geophysical flow fields.

The first experimental data for the flow past a cylinder in a rotating frame was obtained by Boyer (1970) and this work identified three main flow regimes, namely: fully attached flow in which the flow pattern closely approximates that of a potential flow solution; a steady double-eddy regime in which a system of two eddies forms on the downstream side of the cylinder, and finally, an eddy-shedding regime similar to the Kármán vortex street flow in the non-rotating case. Between these three regimes are two transition regions in which the character of the flow alters gradually between that of the neighbouring regimes. The double-eddy system in Boyer's second regime is asymmetric with the larger eddy remaining attached to the cylinder and the smaller eddy lying slightly away from the cylinder. This asymmetry is not observed in the non-rotating flow experiments (and is not present in the parameter regime considered in the present study). Boyer & Davies (1982) completed a further and more extensive experimental study, which included investigation of flows on a β-plane and detailed measurements of the length of the eddy systems as a function of the flow parameters.

Theoretical studies have been carried out by Barcilon (1970) and Walker & Stewartson (1972) for the case when both the Rossby number Ro and the Ekman

number E are small. In the latter study, Walker & Stewartson predicted that boundary-layer separation for the steady flow is dependent on a single parameter $\lambda = Ro/2E^{\frac{1}{2}}$ and would occur for $\lambda \geqslant \frac{1}{2}$, using the results from studies of a similar problem in magnetohydrodynamics (Leibovich 1967; Buckmaster 1969, 1971).

Merkine & Solan (1979) derived the equations for the flow in the $E^{\frac{1}{3}}$ layer in a similar manner to Walker & Stewartson (1972) and integrated these numerically. Their equations included an additional higher-order term which causes asymmetry in the flow with respect to the undisturbed uniform upstream flow. This term was included in an attempt to explain the observed asymmetry of Boyer's (1970) experiments. Merkine & Solan also derived an identical separation criterion to that of Walker & Stewartson.

Later work by Page (1985) examined the $E^{\frac{1}{4}}$-layer flow in detail for $\lambda \leqslant \frac{1}{2}$. Following on from Buckmaster (1971), this study showed that for $0 \leqslant \lambda \leqslant \frac{1}{4}$ the flow is fully attached and regular at the rear stagnation point, but for $\frac{1}{4} < \lambda \leqslant \frac{1}{2}$ the flow develops a singularity near the rear stagnation point and the boundary layer splits into steady viscous and inviscid regions there. Page & Cowley (1988) extended this work, showing that the boundary-layer structure near the stagnation point for $\frac{1}{4} < \lambda \leqslant \frac{1}{2}$ may be described in terms of three asymptotic regions; two inviscid and one viscous.

In a numerical study of the time-varying, viscous, nonlinear flow Matsuura & Yamagata (1985) compared their results for $Ro < 1$ and $E \ll 1$ to the experimental results of Boyer (1970) and Boyer & Davies (1982) with good qualitative agreement between the respective flow patterns for similar parameter values. The numerical results also matched the experimental measurements of the length of the standing eddies in cases where the flow had separated. It was noted that the eddies which form behind the cylinder initially tend to spin down with the flow inside the eddies becoming almost stagnant at steady state owing to the effects of Ekman suction. In some cases, flow which initially separates may become reattached for the same reason. However, the study by Matsuura & Yamagata did not provide diagnostics suitable for the detailed analysis of the separated region of the flow or for comparison with the work of Page (1987).

Page (1987) studied the form of the inviscid interior flow once separation has occurred and included the effects of the $E^{\frac{1}{4}}$ layer on that flow using techniques analogous to those used for Kirchhoff flows in a non-rotating frame. The rotating-flow equivalents of the Euler equations were used to derive a modified Bernoulli equation and the resulting free-streamline problem was solved numerically to calculate the shape of the separated region. In particular, it was shown that in an inviscid flow the vorticity decays exponentially along streamlines as a consequence of Ekman suction and that any region of fluid bounded by closed streamlines (such as the separation bubble) will be stagnant to leading order. The numerical solutions indicated that the length of the bubble will increase monotonically with the parameter $\lambda = Ro/2E^{\frac{1}{2}}$ once $\lambda > \frac{1}{2}$. Comparison with Boyer & Davies' (1982) experiments showed that while qualitative agreement was good, the calculated bubble lengths did not agree with the experimental measurements for large λ. This was thought to be due to viscous effects, neglected in the numerical solution, which are analogous to the $O(R^{-\frac{1}{16}})$ modifications considered by Smith (1979) in his study of the non-rotating, laminar flow past a cylinder at large Reynolds numbers.

Page (1987) also considered higher-order effects on the flow due to the $E^{\frac{1}{4}}$ layers and proposed the form of the separated flow as illustrated in figure 1. Region I here is the irrotional, effectively inviscid, interior flow, region II is inside the separation bubble

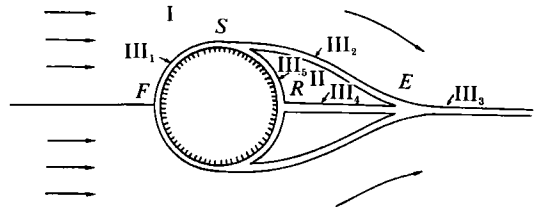

FIGURE 1. Schematic diagram of the form of the separated flow as proposed by Page (1987).

and region III_1 represents the $E^{\frac{1}{4}}$ layer on the surface of the cylinder. The region behind the cylinder is bounded by two free shear layers (region III_2) of thickness $E^{\frac{1}{4}}$, which lie along streamlines for the interior flow. These 'free streamlines' separate from the cylinder at the point S, the position of which is dependent on λ, and move toward the front of the cylinder with larger λ, and join together in a cusp at E, further downstream. The region III_3 forms the wake of the bubble and is also of thickness $E^{\frac{1}{4}}$.

Within the separated region, Page (1987) followed Smith (1985) and proposed that part of the free-streamline flow (region III_2) turns by 180° at E and flows toward the cylinder along the line of symmetry to form a jet (region III_4) which expels fluid into the separated region, causing a flow of $O(E^{\frac{1}{4}})$ in this region. (Similar reversed jets at reattachment of a boundary layer have also been proposed by Messiter, Hough & Feo (1973) and Daniels (1979) in studies of laminar boundary layers in supersonic flows.) The jet (III_4) hits the cylinder and forms another shear layer (region III_5) on the back surface of the cylinder and fluid is thus transported toward the separation point S, at which point the jet would turn and join the lower part of region III_2, proceeding along to the reattachment point E to start the process again.

In this paper, the rotating, viscous flow equations for the cylindrical configuration are solved using a numerical technique and the resulting flow patterns are analysed and compared to Page's (1987) inviscid model. In particular, his proposals regarding the detailed structure of the separated flow, described above, are investigated in the limit as E is decreased.

2. Formulation

Consider the uniform flow, with speed U^* at infinity, past a circular cylinder of radius l^* and axis parallel to $\hat{\boldsymbol{k}}$, placed between two infinite parallel plates a distance d^* apart. The entire system is rotating with a uniform angular velocity $\boldsymbol{\Omega}^* = \Omega^*\hat{\boldsymbol{k}}$ and the axis of rotation is aligned with the axis of the cylinder. This configuration is illustrated in figure 2.

The equations of motion for the flow of a homogeneous, viscous fluid of constant density ρ^* and kinematic viscosity ν^*, relative to the rotating frame, are written in terms of the non-dimensional quantities,

$$\boldsymbol{x} = \boldsymbol{x}^*/l^*, \quad \boldsymbol{u} = \boldsymbol{u}^*/U^*, \quad t = t^*/T^*, \quad d = d^*/l^*, \tag{2.1}$$

where $\boldsymbol{x} = (x, y, z)$ are coordinates measured relative to the rotating frame with z aligned with $\hat{\boldsymbol{k}}$, $\boldsymbol{u} = (u, v, w)$ is the scaled velocity and T^* is a characteristic timescale for the motion. The coordinate x is chosen to lie in the direction of the flow at infinity. The pressure is combined with the centrifugal contribution to form the reduced

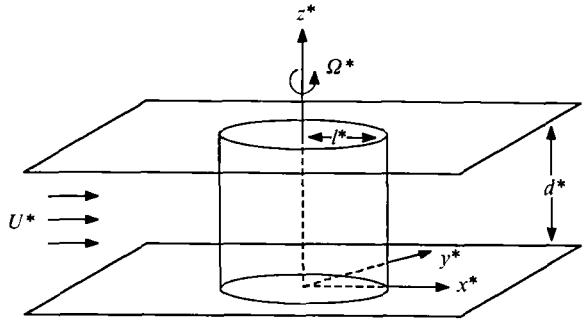

FIGURE 2. Geometrical configuration for the flow past a cylinder in a rotating frame.

pressure $P^* = p^* - \frac{1}{2}\rho^{*2}\Omega^{*2}r^{*2}$, which is then scaled by $\rho^* l^* \Omega^* U^*$. The resulting non-dimensional equations are thus

$$T\frac{\partial \boldsymbol{u}}{\partial t} + Ro(\boldsymbol{u}\cdot\nabla)\boldsymbol{u} + 2\hat{\boldsymbol{k}}\times\boldsymbol{u} = -\nabla P + d^2 E\nabla^2\boldsymbol{u}, \tag{2.2}$$

$$\nabla\cdot\boldsymbol{u} = 0, \tag{2.3}$$

where $T = (T^*\Omega^*)^{-1}$ and the Rossby and Ekman numbers are defined by

$$Ro = \frac{U^*}{\Omega^* l^*}, \quad E = \frac{\nu^*}{\Omega^* d^{*2}}, \tag{2.4}$$

respectively. The boundary condition, $\boldsymbol{u} = 0$ is applied on both the cylinder surface and $z = 0, d$.

Considering E and Ro to be small, the leading-order terms on a long timescale, $T^* \gg \Omega^{*-1}$ are

$$2\hat{\boldsymbol{k}}\times\boldsymbol{u}_0 = -\nabla P \tag{2.5}$$

which implies that the flow is geostrophic and depth independent to lowest order. Since the flow is two-dimensional, a streamfunction ψ can be defined as

$$u = -\frac{\partial\psi}{\partial y}, \quad v = \frac{\partial\psi}{\partial x}, \tag{2.6}$$

in the usual way. To determine ψ, it is most convenient to take the curl of (2.2) yielding the equation for the z-component of vorticity $\zeta = (\nabla\times\boldsymbol{u})\cdot\hat{\boldsymbol{k}} = \nabla_h^2\psi$,

$$T\frac{\partial\zeta}{\partial t} + Ro\left(u\frac{\partial\zeta}{\partial x} + v\frac{\partial\zeta}{\partial y}\right) = (2 + Ro\zeta)\frac{\partial w}{\partial z} + d^2 E\nabla_h^2\zeta, \tag{2.7}$$

where ∇_h^2 is the horizontal Laplacian.

For the flow bounded above and below by parallel plates, the Ekman compatibility conditions (see, for example, Moore 1978) are $w = \frac{1}{2}dE^{\frac{1}{2}}\zeta$ on $z = 0$ and $w = -\frac{1}{2}dE^{\frac{1}{2}}\zeta$ on $z = d$ and hence, using that ζ in (2.7) is independent of z,

$$\frac{\partial w}{\partial z} = -E^{\frac{1}{2}}\zeta. \tag{2.8}$$

For $Ro = O(E^{\frac{1}{2}})$ and choosing $T = (T^*\Omega^*)^{-1} = 2E^{\frac{1}{2}}$, appropriate to the timescale of Ekman-layer dissipation, the governing equations are, to leading order,

$$\frac{\partial \zeta}{\partial t} + \lambda\left(u\frac{\partial \zeta}{\partial x} + v\frac{\partial \zeta}{\partial y}\right) = -\zeta + \delta^2 \nabla_{\mathrm{h}}^2 \zeta, \tag{2.9}$$

$$\nabla_{\mathrm{h}}^2 \psi = \zeta, \tag{2.10}$$

where

$$\lambda = \frac{Ro}{2E^{\frac{1}{2}}} = O(1), \tag{2.11}$$

and

$$\delta = d(\tfrac{1}{2}E^{\frac{1}{2}})^{\frac{1}{2}} \ll 1, \tag{2.12}$$

are the key parameters describing the flow. The viscous term $\delta^2\nabla^2\zeta$ in (2.9), while not of leading order, is retained in the spirit of a composite expansion, since it becomes significant in the boundary-layer region. All other terms of this order are ignored since they remain relatively small everywhere and as a result, the asymmetry noted in Boyer & Davies (1982) and reproduced by Matsuura & Yamagata (1985) is not present in this study. The boundary conditions satisfied by (2.9) and (2.10) are $\psi = \partial\psi/\partial n = 0$ on the cylinder and $\zeta \to 0$, $\partial\psi/\partial y \to -1$ far from the cylinder. Owing to the symmetry noted above, only the flow for $y \geqslant 0$ will be considered from this point.

Equations (2.9) and (2.10) are very similar to those for the equivalent non-rotating flow, (2.9) having only one additional term $(-\zeta)$ on the right-hand side which arises through the effect of Coriolis forces and represents viscous dissipation by Ekman friction.

3. Numerical method

The governing flow equations were solved using a finite-difference technique, but first the exterior of the cylinder was mapped conformally into the upper half plane using the Joukowski transformation $w = \frac{1}{2}(z + 1/z)$ where $z = x + iy$ is the physical plane and $w = \xi + i\eta$ represents the computational domain. This transformation simplifies the application of the boundary conditions since the surface of the cylinder is mapped to the $|\xi| \leqslant 1$ section of the ξ-axis and it also provides better resolution in the far field than, for example, the polar coordinates used by Matsuura & Yamagata (1985) to produce their numerical solutions. Adequate resolution far from the cylinder, particularly in the downstream direction, is important since the purpose of this study is to examine the detailed structure of the separated region of the flow.

In order to resolve the thin, viscous $E^{\frac{1}{4}}$ layer on the cylinder without using excessive computing time, (2.9) and (2.10) were evaluated on a stretched grid which concentrates the grid points near the solid boundary and also near the singular points $w = (\pm 1, 0)$ of the Joukowski transformation. Two separate stretching functions are required: one to stretch the vertical coordinate η to provide adequate resolution within the boundary layer (which is of scale thickness δ), and the other to give a uniform spacing around and close to the cylinder, by stretching the horizontal coordinate ξ. Far from these critical regions, the grid becomes approximately uniform.

Considering first the horizontal coordinate, let s_i, for $i = 0, 1, \ldots, M$ be a set of uniformly spaced grid points on $0 \leqslant s \leqslant 1$. The s_i are divided into three regions: the points in front of the cylinder ($0 \leqslant s_i \leqslant s_{\mathrm{F}}$), those on the cylinder ($s_{\mathrm{F}} \leqslant s_i \leqslant s_{\mathrm{B}}$), and those behind it ($s_{\mathrm{B}} \leqslant s_i \leqslant 1$) where s_{F} and s_{B} are the grid points at $w = (\pm 1, 0)$.

The grids in each of these three regions are transformed by $\xi_i = -\cosh(q_i + \frac{1}{2}\pi)$, $\xi_i = \sin(q_i)$ and $\xi_i = \cosh(q_i - \frac{1}{2}\pi)$ respectively where

$$q_i = \begin{cases} a_1 s_i + b_1/(1-s_i) + c_1 & \text{for } 0 \leqslant s_i \leqslant s_{\mathrm{F}}, \\ a_2 s_i + c_2 & \text{for } s_{\mathrm{F}} \leqslant s_i \leqslant s_{\mathrm{B}}, \\ a_3 s_i + b_2/s_i + c_3 & \text{for } s_{\mathrm{B}} \leqslant s_i \leqslant 1, \end{cases} \tag{3.1}$$

and $-\xi_{\max} \leqslant \xi_i \leqslant \xi_{\max}$. The three functions are made continuous at s_{F} and s_{B} by applying matching boundary conditions on adjacent functions and solving for the constants $a_1, \ldots, c_3$. It is also possible to adjust the proportions of the total number of grid points that will be placed in each of the three regions. Typically, 40% of the points are placed on the cylinder and 30% each side.

The vertical coordinate is transformed by a straightforward exponential stretching function,

$$t_j = \theta_1\left(\frac{\eta_j}{\eta_{\max}}\right) + \theta_2\left[\frac{(\eta_{\max}+1)}{\eta_{\max}}\left(\frac{\eta_j}{\eta_j+1}\right)\right] + \theta_3\left(\frac{1-\exp(-\eta_j/\delta)}{1-\exp(-\eta_{\max}/\delta)}\right), \tag{3.2}$$

where t_j are evenly spaced grid points with $0 \leqslant t_j \leqslant 1$ for $j = 0, 1, \ldots, N$, η is the stretched coordinate, $0 \leqslant \eta \leqslant \eta_{\max}$, and $\theta_1, \theta_2, \theta_3$ are positive constants which can be adjusted to fine-tune the stretching function, provided $\theta_1 + \theta_2 + \theta_3 = 1$. The function (3.2) is dependent on the boundary-layer thickness, δ, so grid points will be placed within the boundary layer to enable adequate resolution of the velocities in that region. In general, $\theta_1 = \theta_2 = \theta_3 = \frac{1}{3}$ was found to give satisfactory results, with 15–20 grid points within the boundary-layer region for typical values of δ. As a consequence of the conformal mapping, the stretching function also provides fine resolution close to the axis of symmetry so that the flow near the reattachment point and wake is resolved accurately. In contrast, the polar grid used by Matsuura & Yamagata (1985) provides poor resolution in these regions.

For most of the results presented in this paper 160 points were used in the horizontal direction and 80 in the vertical. When λ was large (> 8, say) and δ small (< 0.1) the separation bubble is advected far downstream and a finer grid (200×100) was needed. For other parameter ranges, no significant improvement in the results was noted when the finer grid was used.

The vorticity equation (2.9) was solved using an 'alternating directions implicit' method (see, for example, Roache 1982) and the block-tridiagonal matrix obtained from discretizing the Poisson equation (2.10) was inverted using the BLKTRI routine which uses cyclic reduction (Swartztrauber 1974). Timesteps of 0.05–0.1 were used and the scheme was initialized using the irrotational flow solution for the interior region. In all other respects the numerical scheme is similar to that used by Becker & Page (1989) to solve the equations for the viscous flow in a rotating sliced cylinder.

4. Flow trends

Solutions of the flow equations were thus obtained for a range of values of the two key parameters δ, the scaled boundary-layer thickness defined in (2.12), and λ defined in (2.11), which represents the effect on the flow due to the nonlinear advection terms.

Figure 3 shows the streamlines and vorticity contours for values of $\lambda = 0, 1, 2, 4$, and 8 with fixed $\delta = 0.1$. The contour interval for the streamline plots is constant

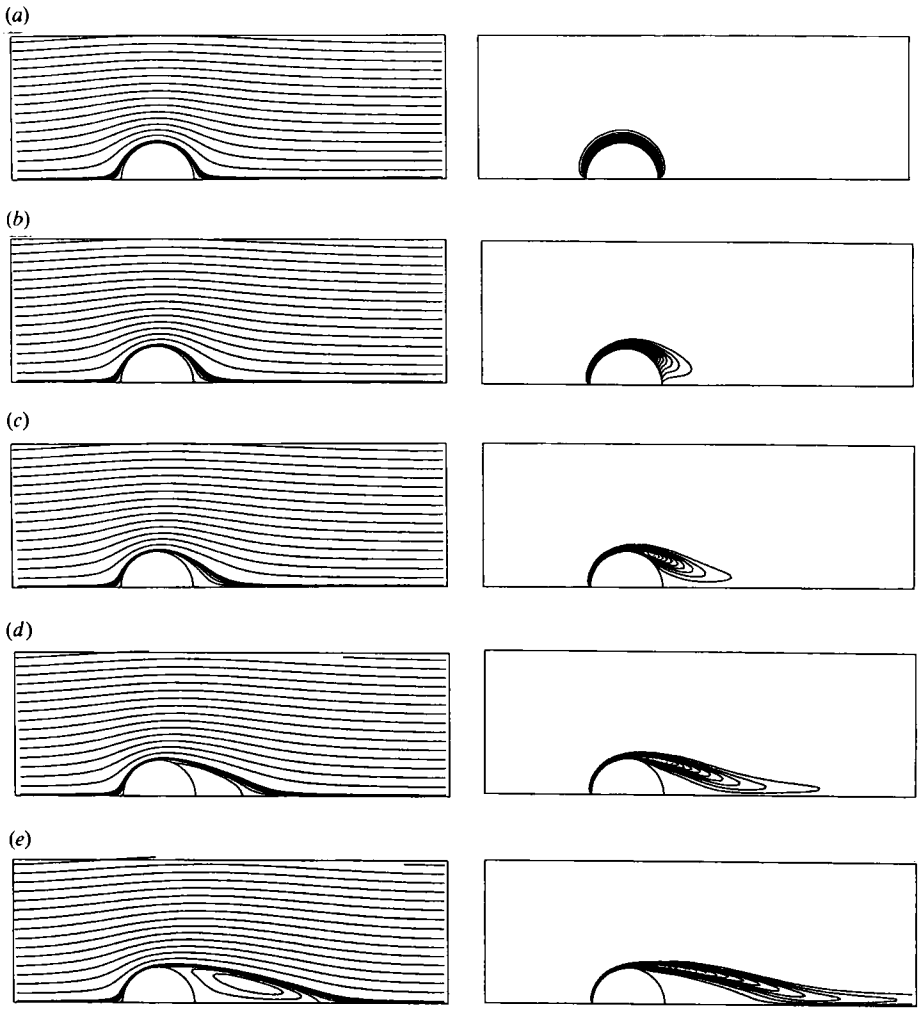

FIGURE 3. Contours of the streamfunction (left) and vorticity (right) for $\delta = 0.1$ and (*a*) $\lambda = 0$, (*b*) $\lambda = 1$, (*c*) $\lambda = 2$, (*d*) $\lambda = 4$, and (*e*) $\lambda = 8$. In each case, the vorticity contour interval is $\Delta\zeta = 0.5$ everywhere and for the streamline is $\Delta\psi = 0.25$ except for $|\psi| \leqslant 0.05$ where it is 0.01.

except near the cylinder (and near the free-streamline in cases for which the flow has separated) where the contour interval has been reduced in order to show some fine details of the flow. The most obvious trend in these plots is the increasing asymmetry about $x = 0$ of the flow patterns with increasing λ. When $\lambda = 0$ the governing equations are linear and advection has no effect on the flow. The streamlines for this value of λ, shown in figure 3(*a*), are symmetric and very similar to those for the potential flow problem. The corresponding vorticity plot shows that vorticity is concentrated in the boundary layer with only a small amount being diffused a small distance from the cylinder into the main flow. When $\lambda = 1$, the streamlines, in figure 3(*b*), are barely asymmetric but the vorticity has already been significantly affected by advection with a noticeable thickening of the boundary layer on the downstream side of the cylinder. The same trend was noted for the attached flow by Page (1985). With λ increased to 2, vorticity has been advected away from the boundary and forms a well-defined wake downstream, although separation has not occurred in the

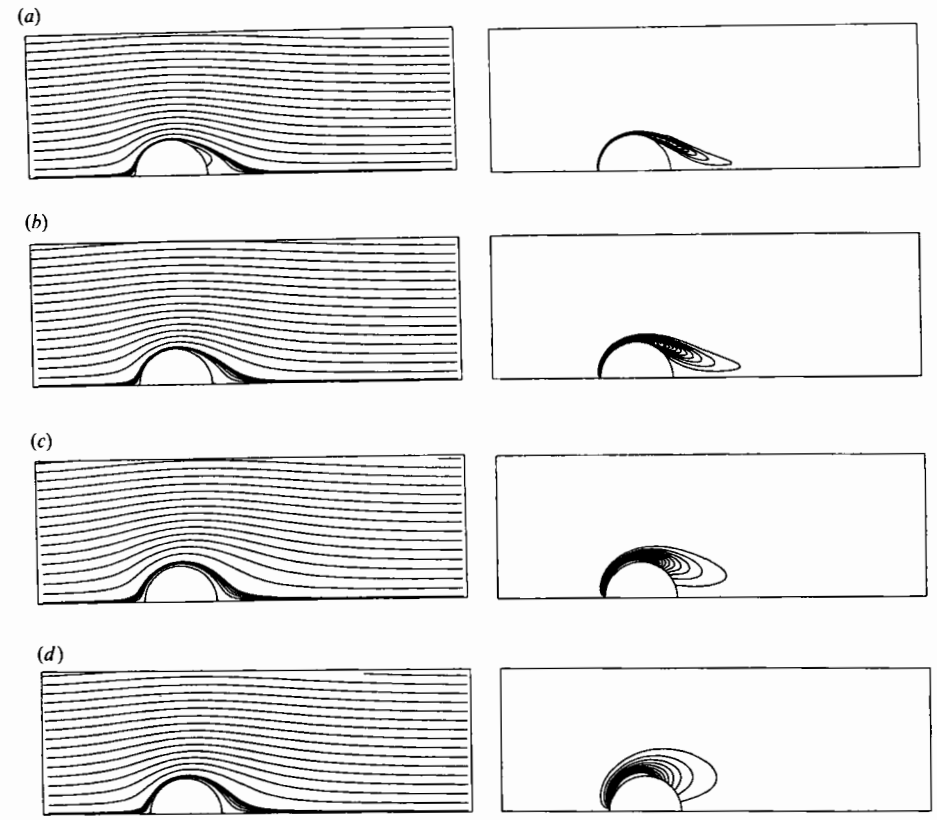

FIGURE 4. Contours of the streamfunction (left) and vorticity (right) for $\lambda = 2$, and (*a*) $\delta = 0.05$, (*b*) $\delta = 0.1$, (*c*) $\delta = 0.2$, and (*d*) $\delta = 0.4$. The contour interval for the vorticity is $\Delta\zeta = 1.0$ for (*a*) and $\Delta\zeta = 0.5$ otherwise. Streamline contour intervals are the same as for figure 3.

sense that reversed flow exists along the cylinder. (For this value of δ the boundary layer separates, in that sense, when $\lambda \approx 2.1$.) The plots for $\lambda = 4$ and $\lambda = 8$ show clearly that the flow has separated and in each case the formation of a separation bubble behind the cylinder is evident in the streamline plots of figure 3(*d*,*e*). The length of this bubble for $\lambda = 8$ is approximately double that for $\lambda = 4$ and the point of separation for $\lambda = 8$ has moved further toward the front of the cylinder compared to the $\lambda = 4$ case. Both of these trends were also noted by Page (1987) and are discussed further in the following section. Inside the separation bubble, it is evident that the flow is relatively slow with some reversed flow present, notably in the case $\lambda = 8$.

A further series of streamline and vorticity contours is shown in figure 4. In this case, the value of $\lambda = 2.0$ is held constant and δ is varied. Again, the contour intervals are constant except very close to the cylinder in the case of the streamfunction plots. These flow patterns are not greatly affected by the change in δ; certainly not to the extent that variations in λ affect the flow. The effect of Ekman suction relative to horizontal diffusive effects and the resulting dissipation of vorticity means that the boundary-layer does not separate until the effective Reynolds number $R \propto Ro/E$ is about 700, or $\delta \approx 0.05$ for this value of λ. The streamlines thus show very little variation from the low-Reynolds-number non-

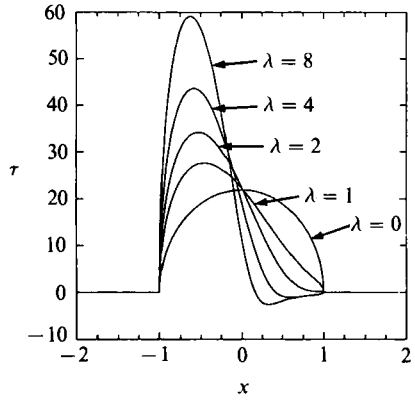

FIGURE 5. Plots of the skin friction for values of $\delta = 0.1$ and $\lambda = 0, 1, 2, 4, 8$.

rotating flow patterns until δ is small enough for separation to occur. The vorticity contours show that vorticity is diffused further into the interior flow for larger δ confirming that the thickness of the boundary is proportional to and of the same magnitude as δ. The effect of advection in sweeping the diffused vorticity downstream remains relatively constant for each of the plots in figure 4, as would be expected since λ is held constant.

A further indicator of the trends in the flow for varying values of the key parameters is the 'skin friction' which is the shearing stress on the surface of the cylinder and is defined by

$$\tau = \left(\frac{\partial u}{\partial y}\right)_{\text{cylinder}}. \tag{4.1}$$

If the flow separates, the point of separation can be determined by the condition that the skin friction vanishes there, since by the definition used here, the separation point is the point at which the zero streamline separates from the surface of the cylinder. The velocity gradient normal to the surface will then be of opposite sign to that occurring before the separation point.

Figure 5 shows a series of plots of the skin friction as a function of x for a range of λ values and fixed $\delta = 0.1$. The parameter values used for figure 5 match those for the contour plots in figure 3. For $\lambda = 0$, the skin friction is symmetric about the y-axis and has the smallest maximum magnitude. With increasing λ, the maximum value of τ increases also since the boundary layer is becoming thinner on the upstream side of the cylinder (see, for example, figure 1 in Page 1985). On the downstream side of the cylinder the plots show a marked trend, with the skin friction decreasing rapidly with larger λ and becoming negative for $\lambda = 4$ and $\lambda = 8$. These two λ values are the only ones for which separation has occurred for the value of δ shown, although the vorticity field in figure 3(*b*) does suggest that the shear layers are not fully attached to the cylinder surface.

It appears both from the plots in figure 5 for $\lambda = 4$ and $\lambda = 8$ and from figure 3 that the boundary layer separates at a point which moves closer to the front of the cylinder as λ increase. This is demonstrated more clearly in figure 6 which shows the separation point s_s in terms of the arc length s, measured from the front stagnation point, for a range of parameter values. (As an indication of the dependence of the numerical results on the resolution used, calculations were also carried out for several

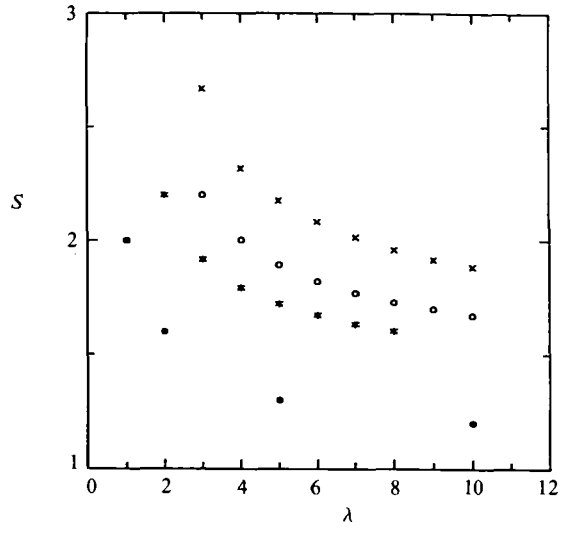

FIGURE 6. Plot showing the variation of the separation point for varying λ with *, $\delta = 0.05$; ○, $\delta = 0.1$; ×, $\delta = 0.2$ from the present study and ●, $\delta = 0$ from Page (1987).

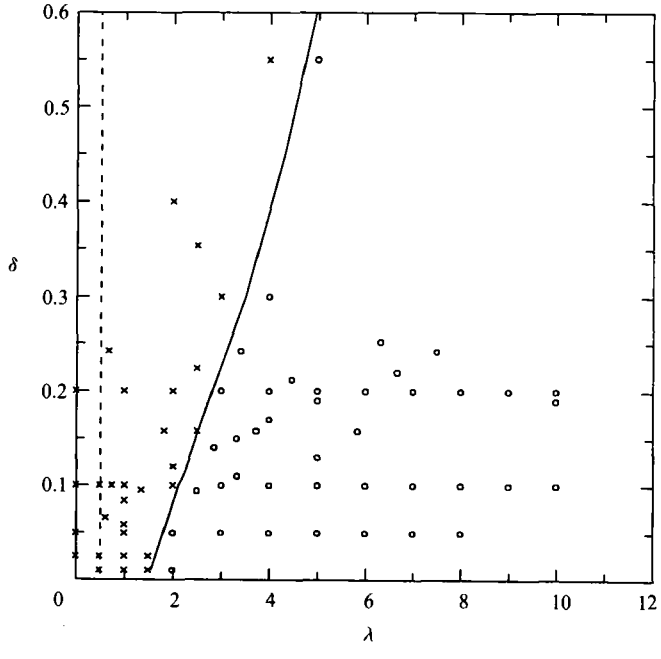

FIGURE 7. Plot of the λ versus δ parameter space: ○, boundary layer has separated; ×, boundary layer not separated; ---, necessary separation criterion predicted by Walker & Stewartson (1972) and Page (1985); ——, separation criterion based on the numerical results of the present study.

different grids, and the difference in s_s between the coarsest grid (80×40) and the finest (160×80) was only 1–3 %). The predictions from Page (1987) for $\delta = 0$ are also shown.

On the basis of figure 6, the separation point moves monotonically towards the front of the cylinder for increasing λ, with δ fixed, and also for decreasing δ, with λ

fixed. In fact, the separation point appears to be approaching a limit as $\lambda \to \infty$, consistent with the prediction of Page (1987) that the separation point should approach $s \approx 0.96$ as $\lambda \to \infty$ for $\delta = 0$. Page (1987) also suggests that the separation point moves towards the rear of the cylinder owing to viscous effects such as the $O(\delta^{\frac{1}{3}})$ modifications considered by Smith (1985, §2.4) and this accords with figure 6 which shows a similar trend for increasing δ.

A plot of the character of the flow as a function of λ and δ is shown in figure 7. Each numerical experiment is shown with a '○' or '×' indicating whether or not the boundary layer has separated, in the sense defined earlier. The dotted line, $\lambda = \frac{1}{2}$ is the necessary criterion for boundary-layer separation to occur, as derived by Walker & Stewartson (1972) and Page (1985). The solid sketched line shows the predicted sufficient separation criterion as a function of δ, based on the numerical results presented here. The solid line should approach the line $\lambda = \frac{1}{2}$ more rapidly than the numerical results indicate for $\delta \to 0$ although this is possibly due to poor numerical resolution of the separated shear layer for small values of δ causing inaccuracy in the results for $\delta = 0.01$ and $\delta = 0.025$. Alternatively, the inconsistency could be due to separation, in the sense of a shear layer leaving the cylinder surface, occurring at a smaller value of λ than that at which τ first vanishes on the cylinder. A similar difficulty in identifying whether separation has occurred in a laboratory study was noted by Boyer & Davies (1982).

5. Comparison with Page's (1987) model

Comparing the results of the present study with the free-streamline calculations of Page (1987) demonstrates a good qualitative agreement in the form of the separated flow. Some differences in the two sets of results are apparent and these may be explained in terms of the viscous effects which are not included in Page's model.

In the study of the inviscid flow, δ is effectively zero, and the flow separates for all $\lambda > \frac{1}{2}$, whereas in the viscous model δ is finite and so, not only will the flow separate at higher values of λ than the inviscid flows, but also the flow patterns will be altered somewhat owing to viscous effects. One immediately obvious effect of viscosity is the smoothing of the streamfunction at the reattachment point – in the inviscid case, the free-streamlines form a cusp at the point of reattachment. Another difference is that separation occurs at a point closer to the front of the cylinder in the inviscid case and this agrees with figure 6 which indicates that the separation point moves forward with decreasing δ values.

The separation bubbles appear to be longer in the inviscid case compared to the equivalent viscous plots and this may be confirmed by examining the data plotted in figure 8 which shows calculated bubble lengths from both Page (1987) and the present study for various δ values. The values of ϵ shown in this diagram are defined to be the distance from the rear of the cylinder to the point where the separation of the two streamlines $\psi = \pm 0.02$ is 0.2. This definition, illustrated in figure 8, is based on that in Boyer & Davies (1982) while the values of $(x_e - 1)$ also shown represent the 'true' bubble length, that is, the point at which the zero streamline reattaches. (Note that the values of ϵ shown here from the inviscid study are actually slightly different from the values shown in figure 5 of Page (1987) since the latter values were calculated from the point at which the bubble half-width is 0.2 rather than 0.1 as defined here.)

Looking at the four sets of data for the bubble length ϵ, it is apparent that ϵ increases approximately linearly with λ in each case and that ϵ also increases with

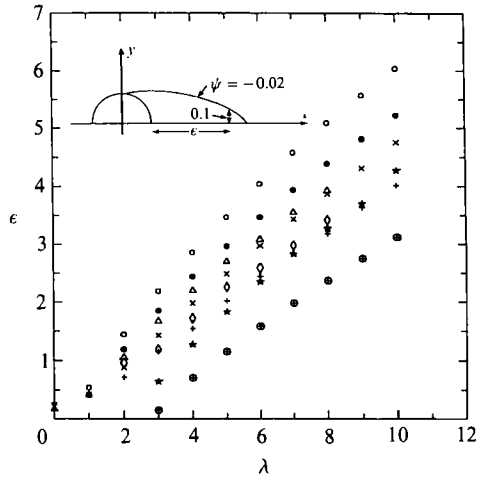

FIGURE 8. Plot of the 'bubble length' ϵ against λ obtained from Page (1987), indicated by the symbol ● and the corresponding values of $(x_e - 1)$ indicated by ○. Results of the present study shown are: bubble lengths for △, $\delta = 0.05$; ×, $\delta = 0.1$; +, $\delta = 0.2$, and the corresponding values of $(x_e - 1)$ for ◇, $\delta = 0.05$, ★, $\delta = 0.01$, ⊕, $\delta = 0.2$. The definition of ϵ is also illustrated.

decreasing δ values. For the smallest value of δ shown, $\delta = 0.05$, the ϵ values (△) are very close to the inviscid values (●). In fact, for small λ, all the ϵ values show reasonable agreement – for $\lambda = 1$ all the ϵ values coincide. With increasing λ, the inviscid bubble lengths diverge from the viscous values, increasing at a greater rate. (Note that because ϵ is measured, as shown in figure 8, based on the $\psi = -0.02$ streamline, it is possible to obtain a 'bubble length' for unseparated cases.)

The values of $(x_e - 1)$ shown on figure 8 are also interesting. In Page (1987) it is clear that $(x_e - 1)$ was greater than ϵ, however the numerical results here show that the zero streamline joins the axis before ϵ. There are two possible reasons for this: first, ϵ here is based on the $\psi = -0.02$ streamline which would be to the right of the $\psi = 0$ streamline near reattachment. Secondly, the $O(\delta)$ flow within the separated region will significantly affect the position of the $\psi = 0$ streamline, since ψ is $O(\delta)$ within both the separated shear layer and the separation bubble.

Figure 9 shows the tangential velocity measured along the streamline $\psi = -3.0$ which is in the interior (inviscid) region of the flow, just outside the boundary layer. The fluid outside the boundary layer accelerates rapidly around the front face of the cylinder attaining its maximum value near the top of the cylinder for $\lambda = 0, 1, 2$ and for $\lambda = 4, 8$, just before the separation point. The velocity then decreases roughly linearly to its minimum point which corresponds to either the rear stagnation point, for the unseparated cases, or the zero streamline reattachment point, for the separated cases $\lambda = 4, 8$. The fluid then increases in velocity to approach the free-stream velocity as $s \to \infty$. These plots are similar in character to the tangential velocities along $\psi = 0$ shown in figure 4 of Page's inviscid study. This similarity is expected since the inviscid solutions represent the flow only in the interior, that is, outside any regions where viscous effects are important such as the boundary layer. Particularly notable is the linear decrease in velocity from the separation point to the reattachment point in the cases $\lambda = 4$ and $\lambda = 8$ and the change in gradient at the reattachment point. In the present study, the velocity gradient is not discontinuous at the reattachment point (as it is in the inviscid study) nor is the velocity zero at

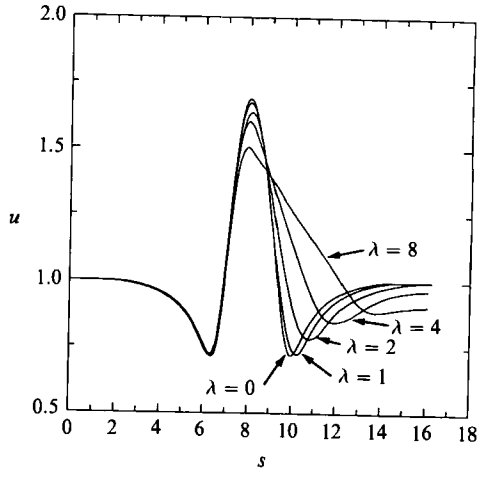

FIGURE 9. Tangential velocity along the streamline $\psi = -0.3$ for $\delta = 0.1$ and varying λ values as shown. The arc-length (s) is measured from the upstream boundary at $x = -8$.

the front of the cylinder due to the smoothing effects of viscosity and the presence of the boundary layer.

6. Detailed structure of the separated flow

In figure 10, a series of flow-speed profiles along coordinate lines in the conformally mapped flow are shown for $\delta = 4$, together with diagrams showing the positions of the profiles. The first profile shows the velocity changing rapidly across the boundary layer from zero on the cylinder to attain the free-stream velocity in the interior region of the flow. The shear across the boundary layer is greater for $\delta = 0.05$ (dashed lines) since for this value of δ the boundary layer is thinner. Profiles 2–6 show a similar increase in velocity across the free shear layer although the gradient is not quite so steep since the shear layer tends to thicken with distance downstream. Below the dots indicating zero velocity on these cross-sections, the profile is crossing the separation bubble and here the velocity is negative and very small in magnitude, increasing to zero on the cylinder surface. On the seventh profile, outside the separation bubble, the velocity is greater than zero everywhere.

These velocity profiles do not support the structure for the separated flow suggested by Page (1987) which included a jet of fluid (identified as III_4 in figure 1) along the line $y = 0$ resulting from some of the fluid in the free shear layer turning 180° at the reattachment point and proceeding in towards the cylinder. The profiles in figure 10 show no evidence of such a jet but rather, suggest that as the fluid in the free shear layer decelerates away from the separation point, it first entrains fluid from inside the separation bubble and then expels this fluid back into the bubble as the shear layer decelerates towards the reattachment point. Thus a region of slow moving, reversed flow is set up inside the bubble as shown in figure 11 (*a*). This flow is of $O(\delta)$, as would be expected of a flow forced by boundary-layer entrainment or detrainment. In contrast, Page (1987) suggested that the net flow inside the bubble should be as shown in figure 11 (*b*), with the inflow from the line $y = 0$ and the cylinder arising from the outflow of the shear layers III_4 and III_5 in figure 1. However, there is little evidence in the numerical solutions to support this proposal.

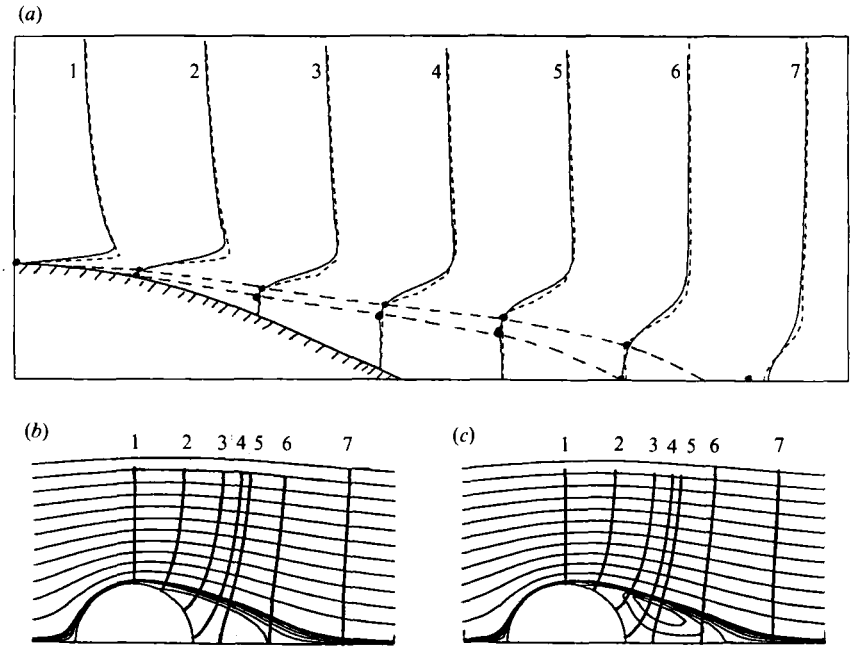

FIGURE 10. (*a*) Velocity profiles along lines of constant x for $\lambda = 4.0$ and ——, $\delta = 0.1$ and – – –, $\delta = 0.05$. The dot on each profile indicates the point at which the velocity is zero and the dashed lines connecting the dots indicate the approximate position of the shear layer. The diagrams below show the positions of the profiles in relation to the cylinder and the separated region of the flow for (*b*) $\delta = 0.1$ and (*c*) $\delta = 0.05$.

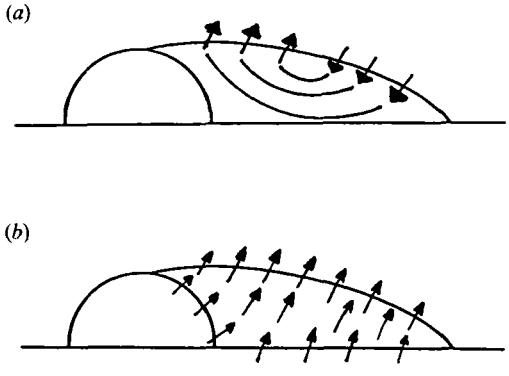

FIGURE 11. Structure of the net flow inside the separation bubble according to (*a*) the present study and (*b*) Page (1987).

7. Conclusions

The viscous model presented in the preceding sections compares well with published experimental results (Boyer 1970; Boyer & Davies 1982) and with other numerical calculations (Matsuura & Yamagata 1985). Comparison with an inviscid model (Page 1987) is also favourable taking into account the variations which are the expected result of viscous effects and does suggest that the theory in that paper does represent a plausible limit for the flow as $\delta \to 0$. In particular, the predictions of the

length of the separation bubble, the position of the separation point and the inviscid velocity on the outer edge of the free shear layer are all consistent with the numerical results presented here. A model of the viscous flow in a different geometrical configuration has been studied also (Becker 1990) and the flows resulting from that model show similar trends although with some interesting variations due to the differing geometry.

In considering the detailed structure of the separated flow past the cylinder, the viscous model has been shown to be inconsistent with the structure proposed in §9 of Page (1987) which was based, in part on the proposed (but as yet unproven) structure for the non-rotating case put forward by Smith (1979, 1985). (It should be noted, however, that the dynamics of the rotating case are altered by Ekman suction which is not present in the non-rotating flows so the conclusions drawn here will not necessarily carry over to the non-rotating flows.) It appears from results presented here that the structure of the flow in the separated region is actually simpler than that suggested by Page, but the precise form of this structure and how it matches in with the free shear layer III_3 will be considered in a later paper (Page & Duck 1990). Further evidence on this question is also provided by Page & Eabry (1989) who conclude that jet flows, such as that in region III_4 of figure 1, lose all of their mass and momentum after a finite distance and consequently that region III_4, if it exists, may terminate a short distance from the reattachment point.

The author wishes to thank Dr M. A. Page for suggesting the problem and for many helpful discussions during its development.

REFERENCES

BARCILON, V. 1970 Some inertial modifications of the linear viscous theory of steady rotating fluid flows. *Phys. Fluids* **13**, 537–544.

BECKER, A. 1990 The flow past a normal flat plate in a rotating frame. *Q. J. Mech. Appl. Maths.* (submitted).

BECKER, A. & PAGE, M. A. 1990 Flow separation and unsteadiness in a rotating sliced cylinder. *Geophys. Astrophys. Fluid Dyn.* (in press).

BERGER, E. & WILLE, R. 1972 Periodic flow phenomena. *Ann. Rev. Fluid Mech.* **4**, 313–340.

BOYER, D. L. 1970 Flow past a circular cylinder in a rotating frame. *Trans ASME* D: *J. Basic Engng* **92**, 430–436.

BOYER, D. L. & DAVIES, P. A. 1982 Flow past a circular cylinder on a β-plane. *Phil. Trans. R. Soc. Lond.* A **306**, 533–556.

BUCKMASTER, J. 1969 Separation and magnetohydrodynamics. *J. Fluid Mech.* **38**, 481–498.

BUCKMASTER, J. 1971 Boundary layer structure at a magnetohydrodynamic rear stagnation point. *Q. J. Mech. Appl. Maths* **24**, 373–386.

DANIELS, P. G. 1979 Laminar boundary-layer reattachment in supersonic flow. *J. Fluid Mech.* **90**, 289–303.

LEIBOVICH, S. 1967 Magnetohydrodynamic flow at a rear stagnation point. *J. Fluid Mech.* **29**, 401–413.

MATSUURA, T. & YAMAGATA, T. 1985 A numerical study of a viscous flow past a circular cylinder on an f-plane. *J. Met. Soc. Japan* **63**, 151–166.

MERKINE, L. & SOLAN, A. 1979 The separation of flow past a cylinder in a rotating system. *J. Fluid Mech.* **92**, 381–392.

MESSITER, A. F., HOUGH, G. R. & FEO, A. 1973 Base pressure in laminar supersonic flow. *J. Fluid Mech.* **60**, 605–624.

MOORE, D. W. 1978 Viscous effects. In *Rotating Fluids in Geophysics* (ed. P. H. Roberts & A. M. Soward). Academic.

MORKOVIN, M. V. 1964 Flow around circular cylinder – a kaleidoscope of challenging fluid phenomena. *Symp. on Fully Separated Flows*, pp. 102–118. ASME.

PAGE, M. A. 1985 On the low-Rossby-number flow of a rotating fluid past a circular cylinder. *J. Fluid Mech.* **156**, 205–221.

PAGE, M. A. 1987 Separation and free-streamline flows in a rotating fluid at low Rossby number. *J. Fluid Mech.* **179**, 155–177.

PAGE, M. A. & COWLEY, S. J. 1988 On the rotating-fluid flow near the rear stagnation point of a circular cylinder. *J. Fluid Mech.* **194**, 79–99.

PAGE, M. A. & DUCK, P. W. 1990 The structure of separated flow past a circular cylinder in a rotating frame. *Geophys. Astrophys. Fluid Dyn.* (to appear).

PAGE, M. A. & EABRY, M. D. 1989 The breakdown of jets in a low-Rossby-number rotating fluid. *J. Engng Maths* (in press).

ROACHE, P. J. 1982 *Computational Fluid Dynamics*. Hermosa.

SMITH, F. T. 1979 Laminar flow of an incompressible fluid past a bluff body: the separation, reattachment, eddy properties and drag. *J. Fluid Mech.* **92**, 171–205.

SMITH, F. T. 1985 A structure for laminar flow past a bluff body at high Reynolds number. *J. Fluid Mech.* **155**, 175–191.

SWARTZTRAUBER, P. N. 1974 A direct method for the discrete solution of separable elliptic equations. *SIAM J. Numer. Anal.* **11**, 1136–1150.

WALKER, J. D. A. & STEWARTSON, K. 1972 The flow past a circular cylinder in a rotating frame. *Z. angew Math. Phys.* **23**, 745–752.